Heliyon 10 (2024) e31226

Contents lists available at ScienceDirect

Heliyon

journal homepage: www.cell.com/heliyon

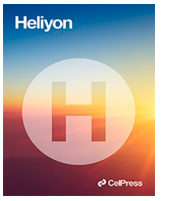

Research article

Sedimentary records of sea level fall during the end-Permian in the upper Yangtze region (southern China): Implications for the mass extinction

Xiong Duan [a,b,*], Zhiqiang Shi [b,**]

[a] School of Geographical Sciences, Sichuan Provincial Engineering Laboratory of Monitoring and Control for Soil Erosion in Dry Valley, China West Normal University, Nanchong, 637009, China
[b] State Key Laboratory of Oil and Gas Reservoir Geology and Exploitation, Institute of Sedimentary Geology, Chengdu University of Technology, Chengdu, 610059, China

ARTICLE INFO

Keywords:
End-Permian
Sea level fall
Upper Yangtze region
Mass extinction

ABSTRACT

Sea level fall is considered one of the significant factors leading to the end-Permian mass extinction (EPME). We studied the relative sea level changes in the Beifengjing and Shangsi sections, and the results indicate that a sea level fall occurred in the Upper Yangtze region during the Permian–Triassic transition. Considering that there is no significant change in fossil abundance in the strata following the two sea level falls observed in the Beifengjing section, we conclude that the reduction in shallow marine habitat for sea level fall solely was insufficient to cause the mass extinction. However, sea level fall did exacerbate the input of terrestrial debris into the ocean, leading to the deterioration of the marine environment. We propose that the combined adverse effects of volcanic eruptions, sea level falls, and other events exceeded the threshold for biological survival, ultimately resulting in the catastrophic EPME.

1. Introduction

During the Permian–Triassic transition, the Earth experienced the most severe mass extinction event since the Cambrian explosion [1,2], resulting in approximately 49 % and 81 % losses of marine taxa at the family and species levels, respectively [2,3], as well as varying degrees of impact on terrestrial organisms [2,4–6]. Recent breakthroughs in research on the end-Permian mass extinction (EPME) event in many fields such as geochronology, geochemistry, geophysics, mineralogy, paleontology, sedimentology, stratigraphy, and paleomagnetism have led to a complex and multifactorial extinction theory [7–9]. Previous studies on the global climate background and marine environment during the Permian–Triassic transition have shown that the direct causes of the mass extinction were manifold, including oceanic anoxia [1,10–17], climate warming [18–22], atmospheric ozone depletion [23–26], ocean acidification [27–30], marine poisoning [31–35], and extraterrestrial impact [36–38]. However, the hypothesis of extraterrestrial impact remains heavily disputed owing to the lack of conclusive evidence during the Permian–Triassic boundary (PTB) crisis [39,40]. Increasingly, scholars believe that the volcanic activity of the Siberian Large Igneous Province may be the main driving force for direct

* Corresponding author.School of Geographical Sciences, Sichuan Provincial Engineering Laboratory of Monitoring and Control for Soil Erosion in Dry Valley, China West Normal University, Nanchong, 637009, China.
** Corresponding author.
E-mail addresses: duanxiong00@163.com (X. Duan), szqcdut@163.com (Z. Shi).

https://doi.org/10.1016/j.heliyon.2024.e31226
Received 5 February 2024; Received in revised form 10 May 2024; Accepted 13 May 2024
Available online 14 May 2024

harm to biota [9,41–46]. Dating back to the times before the 1990s, sea level change, was proposed as the primary cause for the EPME for decades [47–50]. In 1989, Hallam reviewed previous work on sea level fall and suggested that the mass extinction was caused not by regression, but by the spread of anoxic bottom seawater and subsequent transgression [51]. Clarifying the sea level changes at the Permian–Triassic transition is of great significance for studying the most severe mass extinction event since the emergence of complex life owing to its wide-ranging regional impact, long-lasting effects, and direct consequences on sedimentary environment changes and species replacement [52].

The most direct manifestation of sea level rise and fall can be observed in the changes in the proportions of ocean and land areas relative to the total global area [53]. From the Early Permian to Changhsingian, the global shallow marine area decreased sharply from 43 % to 13 %, but it increased again to 34 % in the Early Triassic [48]. This indicates that global regression reached its peak in the Late Permian, and a new phase of transgression occurred in the Early Triassic. In the 1980s, with the development of sequence stratigraphy theory, the regression during the Late Permian and the transgression during the Early Triassic were further explored [54,55]. Subsequently, many scholars believed that the regression ended tens of centimeters or several meters below the PTB, and the new transgression had begun at the latest Permian, rather than at the earliest Triassic [56–59]. However, in basin or slope environments, it is possible that the relatively deeper water and limited magnitude of sea level fall result in a lack of direct evidence of exposure. As a result, the existence of sea level fall events may have been overlooked, which is a thought-provoking issue [60–62]. When studying the PTB strata in the southern China, especially in shallow-water carbonate platform depositional areas, it is common to find lithological boundary transitions several decimeters to meters below the PTB. In the Laolongdong section, the uppermost part of the Upper Permian is characterized by reef limestone, whereas the lowermost part of the Lower Triassic is successively deposited with micrites and microbialites [62,63], as well as two sea level falls approximately 0.4 m above and below the PTB [62]. In the Xiushui section, 2 m thick microbialite overlies uppermost Permian bioclastic limestone [64]. Yin et al. reviewed more than 20 PTB sections in southern China and pointed out that in shallow-water carbonate platforms, Changxing limestone is often covered by several meters thick Upper Triassic carbonate microbial rocks [65].

In this study, we selected the Beifengjing section in Shapingba, Chongqing in shallow water deposition and the Shangsi section in Guangyuan, Sichuan, in deep-water deposition as the research objects. We conducted comprehensive studies of sedimentology, as well

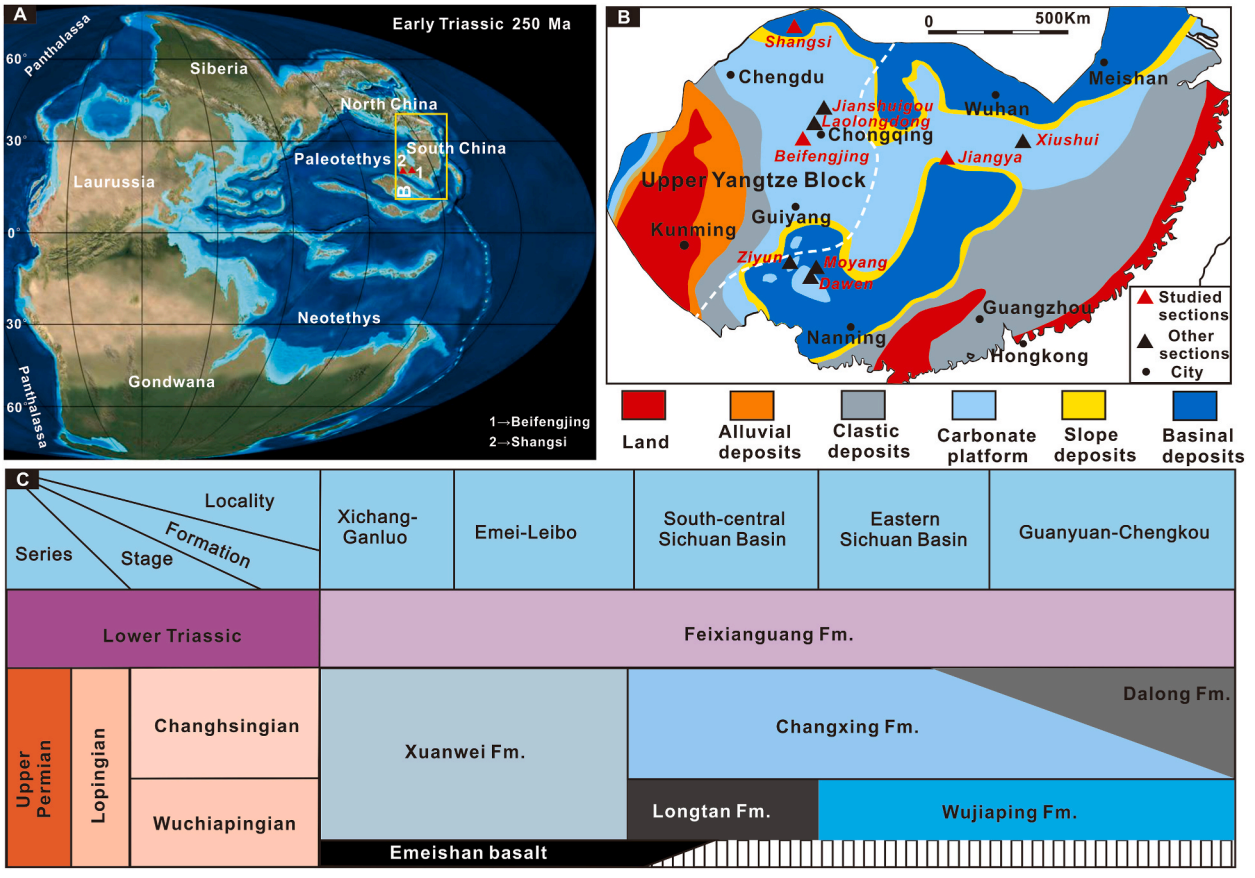

Fig. 1. Late Permian–Early Triassic paleogeographic map and stratigraphic system of the study area. A, Paleogeography of the world during the Early Triassic (modified from Ref. [71]), 70° counterclockwise of South China craton relative to its modern orientation; B, Paleogeographic map (solid yellow box in panel A) showing the study sites (modified from Refs. [65,72]); C, Simplified chart illustrating the Upper Permian and Lower Triassic stratigraphic systems of the Upper Yangtze region (modified from Ref. [73]). Fm. = Formation.

as wavelet analysis based on gamma data and Fischer plot, to clarify the changes in sea level in the Upper Yangtze region during this period.

2. Geologic setting and studied sections

During the Late Permian, strong rifting movements led to the peak eruption of Emeishan basalt, which was called the "Emei Taphrogenesis" and had a profound impact on the paleogeographic pattern of the Upper Yangzi region during the Late Permian and Early Triassic [66]. There is a significant differentiation of sedimentary facies zones in the Late Permian–Early Triassic of the Upper Yangtze region (Fig. 1A and B). The deep-water trough facies zone is primarily composed of dark-colored, thin-bedded siliceous rocks, siliceous mudstones, and siliceous limestones, whereas the shallow-water platform facies zone is characterized by bioclastic limestone and biogenic reef limestone deposition [67]. The Changxing Formation, as the uppermost lithostratigraphic unit of the Permian, generally refers to the carbonate platform sediments below the Lower Triassic in the South China region, which are approximately contemporaneous with the Dalong Formation (Fig. 1C). The sedimentary region of the Dalong Formation is also referred to as the "siliceous detrital basin" [68]. The Lower Triassic Feixianguan Formation is widely developed in the study area and is in conformable contact with the underlying Changxing Formation/Dalong Formation. Based on the analysis of paleobiological fossils and carbon isotopes, the age of the Feixianguan Formation corresponds approximately to the Induan stage [69,70].

The Beifengjing section is located in Shapingba District, approximately 15 km southwest of Chongqing City center. Its geographical coordinates are 29°29′30″N latitude and 106°24′06″E east longitude (Fig. 1B). It is tectonically located on the eastern side of the southern Zhongliangshan anticline in the Huayingshan fault zone. The upper part of the Changxing Formation is mainly deposited with clastic limestone, whereas the lower part of the Feixianguan Formation is mainly deposited with micrite and mudstone.

The Shangsi section is located approximately 2 km north of Shangsi Township, Jiange County, Guangyuan City, and tectonically belongs to the southeast wing of the Kuangshanliang anticline in the Indochinese fold belt of the northern segment of Longmen Mountain, with geographical coordinates of 105°30′25″E and 32°17′36″N (Fig. 1B). The upper part of the Upper Permian Wujiaping Formation is thick-bedded micrite, which is conformably in contact with the overlying Dalong Formation. The Dalong Formation mainly deposited micrite, siliceous rock, siliceous limestone, radiolarian chert, siliceous shale and tuff. The lower part of the Feixianguan Formation is mainly deposited mudstone, limestone, muddy-limestone, micrite and conglomeratic limestone. The Shangsi section was once considered one of the candidate sections for the Global Stratotype Section and Point (GSSP) of the PTB, with good exposure and continuous deposition. Furthermore, considerable work has been conducted by predecessors in sedimentology, geochemistry, paleomagnetism and paleontology [57,74–80].

3. Materials and methods

3.1. Conodont data collection

In this study, 56 rock samples were collected from the Shangsi and Beifengjing sections for sedimentological and paleontological research. The rock samples were made into thin sectionsand photographed using an optical microscope (Nikon Lv100 pol).

In addition, 18 rock samples, each weighing approximately 3 kg, were collected from the Beifengjing section for conodont biostratigraphy research. The process of obtaining conodont samples is as follows: 1) The collected rock samples were crushed into particles with a diameter of 1–2 cm indoors, placed in plastic containers, labeled according to field records, and then soaked in 10–20 % industrial acetic acid. The samples were rinsed and the acid was replaced approximately every week for approximately five to six cycles. Subsequently, the acid-insoluble residues were sieved using a 160-mesh sieve and then dried in an experimental oven at 80 °C–90 °C. 2) The dried residues were examined under a binocular microscope to select conodonts. These conodonts were then fixed on carrier plates previously coated with a thin layer of latex using a brush. Finally, the carrier plates were placed under a scanning electron microscope (SEM) for imaging of each sample. All the above work was conducted at the State Key Laboratory of Oil and Gas Reservoir Geology and Exploitation at Chengdu University of Technology.

3.2. Raw gamma data acquisition

Rocks generally contain varying amounts of radioactive elements such as uranium (U) and thorium (Th) and continuously emit radiation. Natural gamma data can be obtained from instrumental measurements of the natural gamma-ray intensity of rocks. Owing to the strong adsorption capacity of clay minerals for radioactive elements, the natural gamma-ray intensity of rocks is directly proportional to the clay content. The clay content in sedimentary rocks is influenced by the depositional environment. For instance, in environments with rising sea levels and weak hydrodynamic conditions, the clay content is higher, and vice versa.

The steps to obtain natural gamma data are as follows: 1) A fresh surface of the rock samples on the field outcrop was taken at equal intervals of 0.2 m using a geological hammer. Then, 2) a portable gamma energy spectrum detector (model GR135) was used to align the fresh surface of the rock for data acquisition, with a sampling time of not less than 60 s. Finally, the gamma value (measured in API units) was recorded after the data were stable. A total of 688 data points were collected from the top of the Upper Permian Wujiaping Formation to the bottom of the Upper Triassic Feixianguan Formation, spanning a stratigraphic thickness of 137.4 m.

3.3. Wavelet analysis and Fischer plot

The natural gamma curve is formed using multiple signals of different frequencies superimposed together. However, if the original gamma curve is used to directly analyze the sedimentary environment and divide the sedimentary sequence, there may be a large error. The common means is to transform the original gamma signal using wavelet analysis. After the gamma signal is processed by wavelet transform, several signal features of different frequencies can be obtained. The signal mutation point of each frequency represents the upper sequence mutation interface on different time scales. Therefore, the sea level change on different time scales can be obtained. The common wavelet types are Haar, Daubechies (abbreviated as dbN, where N refers to the wavelet order), Hymlets, Morlet and Coiflets. The results produced by choosing different wavelet functions to transform are also different. Zhao Wei et al. concluded that db5 wavelet has good applicability in dividing sedimentary cycles by comparing the morphology of wavelets with the morphology of logging curves and analyzing the results of different wavelet transforms [81]. In this study, the raw gamma signal is denoised using Matlab R2018b software, and then the natural gamma curve of the Shangsi section is transformed using the db5 wavelet, and the deposition cycles are divided according to the transformation results.

The Fischer plot is a graphical method used to represent sedimentary facies changes over time. Instead of the traditional one-dimensional lithological columnar diagram, the Fischer plot is a two-dimensional graph with time as the horizontal axis and space–vertical as the vertical axis (Fig. 2A). Later, Sadler et al. improved this method by using the cycle number as the horizontal axis and cumulative departure from the mean cycle thickness (the cumulative sum of the differences between the thickness of each cycle and the average thickness of all cycles) as the vertical axis to create a curve plot [82]. This curve represents the trend of accommodation space changes. After correcting for sedimentation rates, the resulting Fischer plot can be considered as a sea level change curve (Fig. 2B). The reliability of the Fischer plots depends largely on the accuracy of identifying stratigraphic cycles. Sadler et al. recommended using data from the thickness of at least 50 sedimentary cycles to obtain a reasonable Fischer plot [82].

4. Results

4.1. Sedimentary characteristics of the Beifengjing section

The Beifengjing section exposes the upper part of the Changxing Formation and the lower part of the Feixianguan Formation. The total thickness of the Beifengjing section is approximately 9 m, with the Changxing Formation having a thickness of approximately 2.3 m and the Feixianguan Formation having a thickness of approximately 6.7 m. The Beifengjing section is divided into 15 beds from top to bottom (Fig. 3).

Beds 1 to 3 of the Changxing Formation are primarily composed of medium-thick-bedded bioclastic limestone, with subordinate mudstone and tuff (Fig. 3B). Bed 1 is a gray bioclastic limestone with undulating topography and is covered by a paleosol bed. Under the microscope, it reveals fossils such as gastropods, brachiopods, echinoderms, sponge spicules, fusulinids, bivalves, crinoids, and foraminifers (Fig. 4A–D). Bed 2 consists of bioclastic limestone, with severe dissolution occurring in the upper part and filled with paleosols (Fig. 3B). Fossil assemblages in this bed include gastropods, bivalves, fusulinids, and crinoids (Fig. 4E–G).In addition, conodonts (*Clarkina changxingensis* and *Clarkina* sp. *Indeterminate*) have been found within bed 2 (Fig. 5). Bed 3 is a thick tuff, approximately 7 cm in thickness, without observable biogenic fossils, and serves as the boundary between the Changxing Formation and the Feixianguan Formation.

The Feixianguan Formation (beds 4 to 15) is primarily characterized by fine-grained rock sediments, such as limestone, muddy-

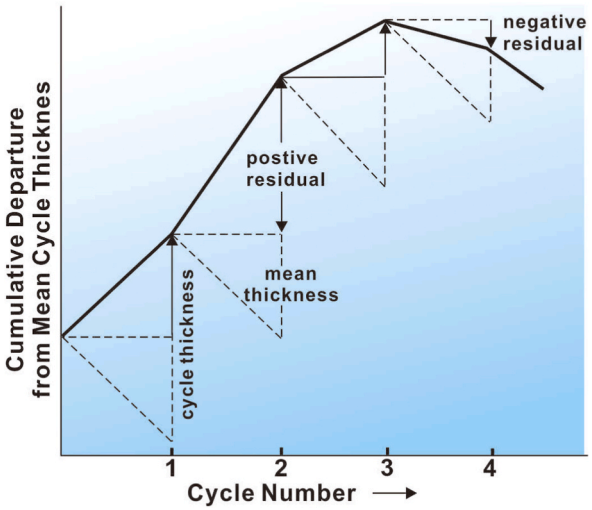

Fig. 2. Cumulative departure from mean cycle thickness as a function of cycle number (Fischer plot) (modified from Ref. [82]).

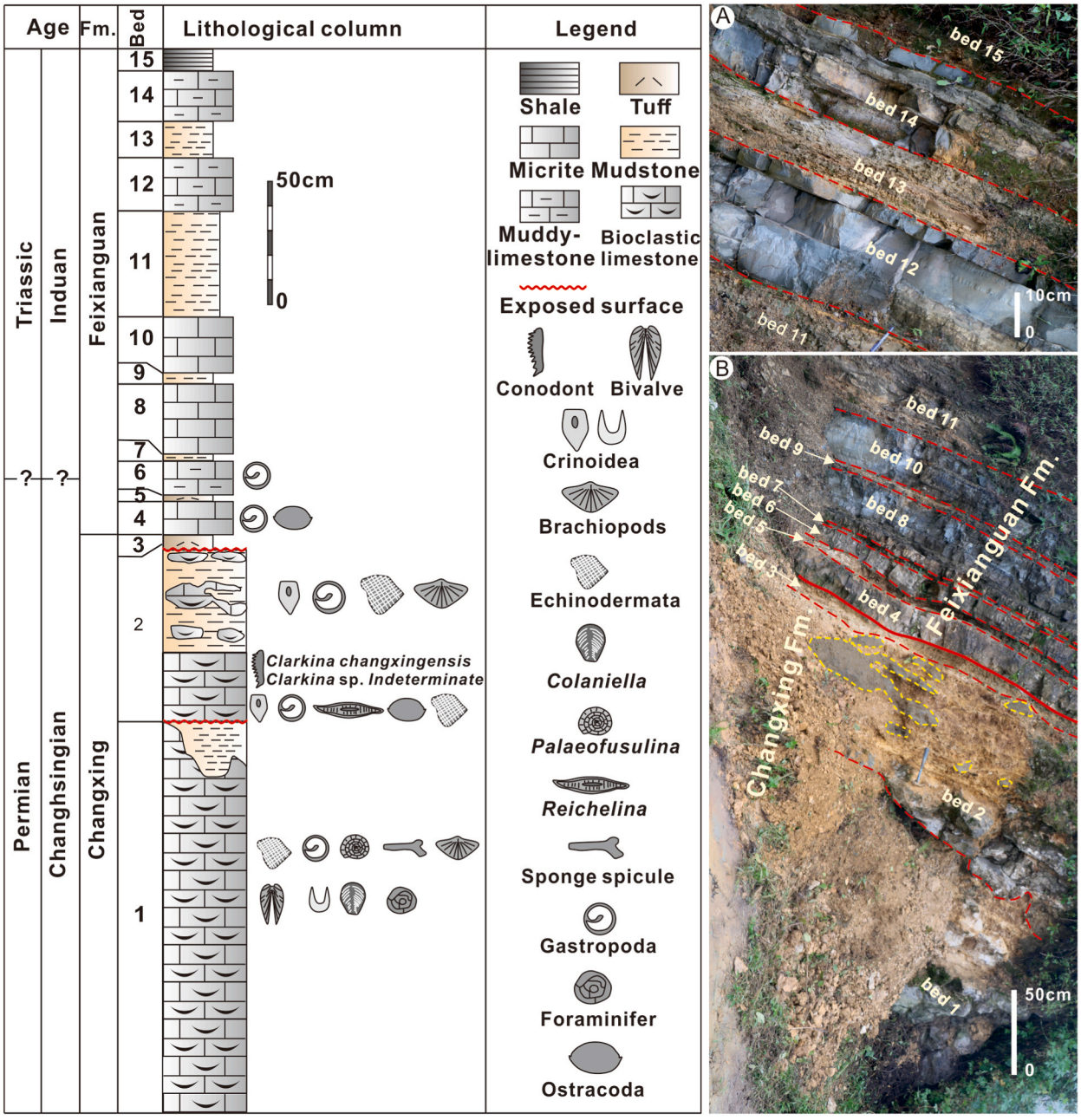

Fig. 3. General lithological column and field outcrop photograph of the Upper Permian–Lower Triassic succession at the Beifengjing section in Chongqing. A, Field macroscopic photographs of beds 1 to 11; B, Field macroscopic photographs of beds 11 to 15. In both panels A and B, the solid red line is the boundary between the Changxing Formation and the Feixianguan Formation, the dotted red line is the boundary between beds, and the dotted yellow line in bed 2 is the residual bioclastic limestone after dissolution. Fm. = Formation.

limestone, calcareous mudstone, mudstone, and shale (Fig. 3A and B). The overall fossil content in this formation significantly decreases. However, beds 4 and 6 still contain a small amount of bioclastic debris (Fig. 4H and I).

4.2. Sedimentary characteristics, wavelet analysis and Fischer diagram of Shangsi section

4.2.1. Sedimentary characteristics

The Upper Permian to Lower Triassic succession at the Shangsi section includes the upper part of the Wujiaping Formation, the Dalong Formation, and the lower part of the Feixianguan Formation, with a total thickness of approximately 137 m (Fig. 6). The Shangsi section in Guangyuan is enriched with diverse fossil groups, including diverse biota such as foraminifers, fusulinids, ostracods,

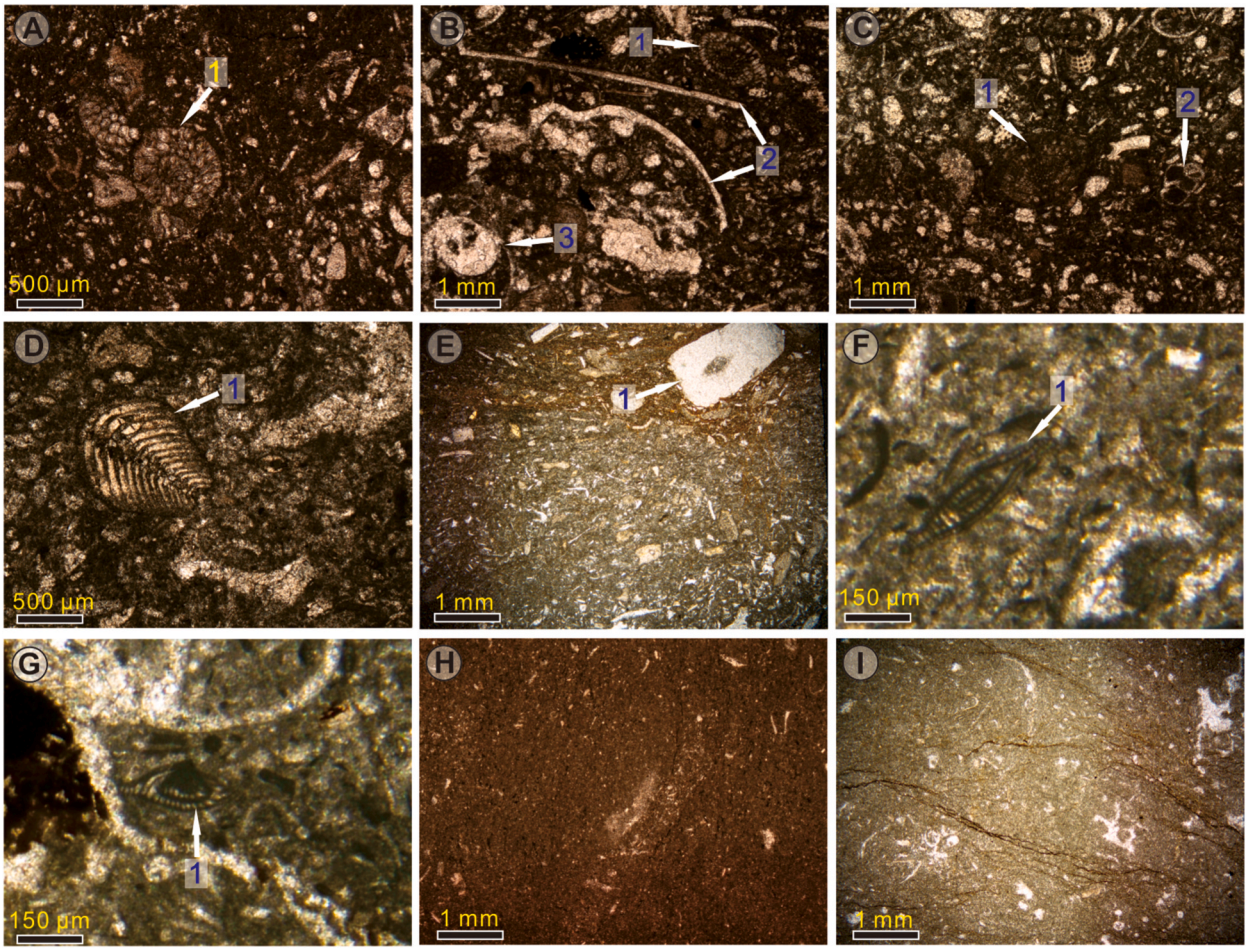

Fig. 4. Microphotographs from the Beifengjing section. A (bed 1), 1 = fusulinid (*Palaeofusulina*); B (bed 1), 1 = fusulinid (*Codonofusiella*), 2 = bivalve biological fragments that have been replaced by calcite, 3 = gastropoda; C (bed 1), 1 = fusulinid (*Palaeofusulina*), 2 = foraminifera; D (bed 1), 1 = foraminifera (*Colaniella*); E (bed 2), 1 = single crystal structure of a crinoid stem plate, with clear axial canal; F (bed 2), 1 = fusulinid (Reichelina); G (bed 2), 1 = fusulinid (*Reichelina*); H (bed 4), Micrite, containing a small amount of bioclasts; I (bed 6), Micrite, containing few bioclasts.

Fig. 5. Conodonts from bed 2 at Beifengjing. 1, *Clarkina changxingensis*; 2–4, *Clarkina* sp. *Indeterminate*. All samples are Pa elements and each scale bar equals 100 μm.

bivalves, ammonoids, crinoids, radiolarians, and conodonts. The distribution of these fossils on the section is closely related to water depth variations. Planktonic organisms are predominantly found in the Dalong Formation, whereas benthic organisms are more abundant in the Feixianguan Formation. In terms of biostratigraphy, Zhang et al. initially established four conodont zones from bottom

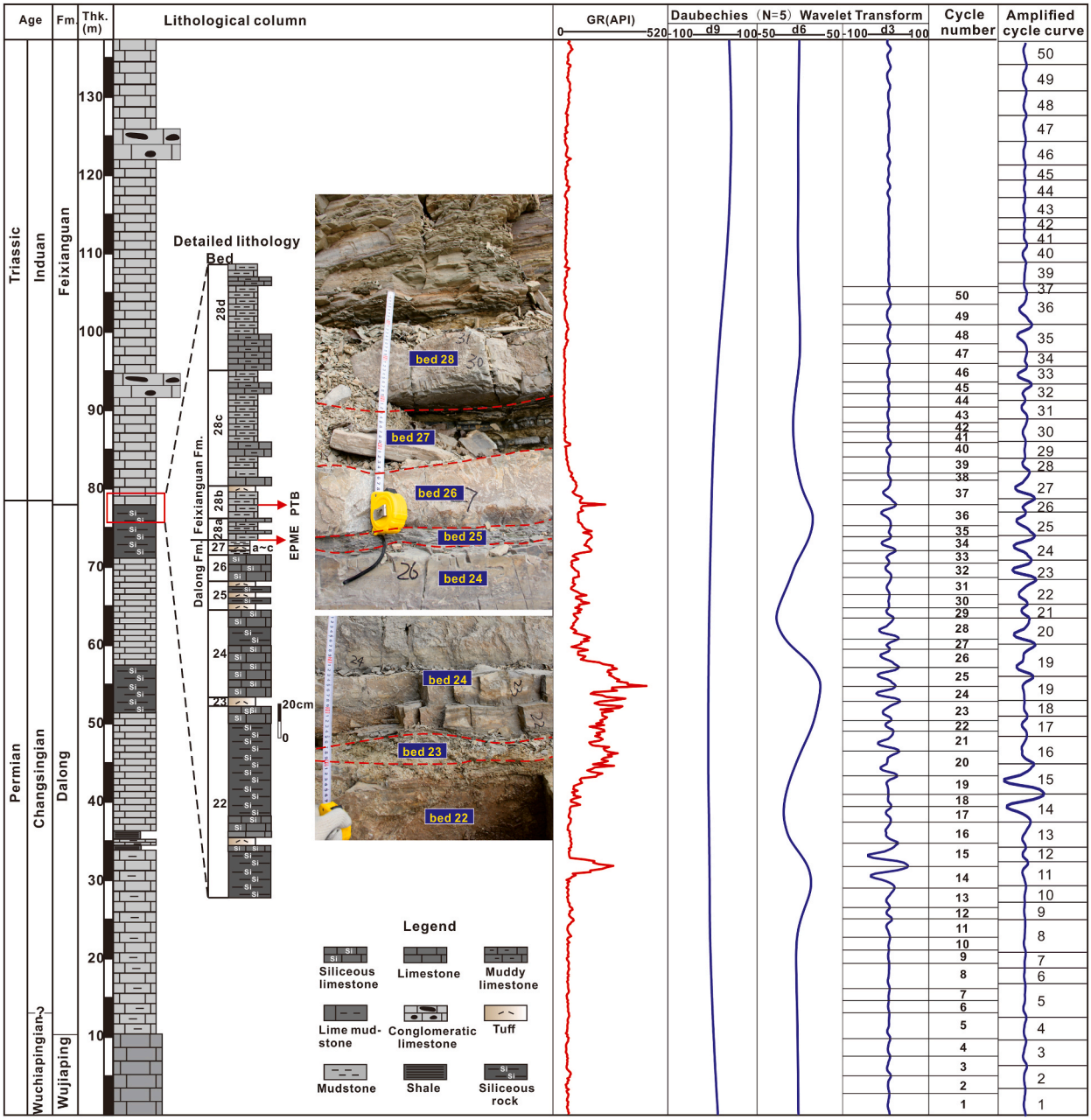

Fig. 6. General lithological column and field outcrop photograph of the Upper Permian–Lower Triassic succession at the Shangsi section in Guangyuan, Sichuan. Fm. = Formation; Thk = Thickness.

to top: *Neogondolella changxingensis–N. subcarinata* Zone, *Anchignathodus* (corresponding to *Hindeodus*) *decrescens* Zone, *A. parvus* Zone, and *Isarcicella isarcica* Zone [75]. Based on this, Jiang et al. revised the four conodont zones as the *Hindeodus changxingensis* Zone, the *H. parvus* Zone, the *I. lobata* Zone, and the *I. isarcica* Zone [80]. The first occurrence of *H. parvus* is situated approximately 20 cm above the base of the Feixianguan Formation (Fig. 6), marking the biostratigraphy boundary between the Permian and the Triassic.

Near the PTB (beds 22–28), we conducted detailed sedimentological research (Fig. 6), and the bed numbers follow the scheme of Jin and Huang [73]. The upper part of the Upper Permian Dalong Formation (beds 22–27) mainly consists of radiolarian chert, tuff, siliceous limestone, and mudstone. Beds 22, 24, and 26 are radiolarian chert, with abundant siliceous radiolarian fossils observed under a microscope (Fig. 7A–C). Bed 23 is tuff, whereas bed 25 is an interbedding of siliceous limestone and tuff. Bed 27 is composed of gray-black mudstone (bed 27a) at the bottom, followed by gray-white tuff (bed 27b) and gray-black mudstone (bed 27c) toward the top. This bed contains only Permian conodont fossils (Fig. 7D) and microspheres (Fig. 7E). The boundary between beds 27 and 28 corresponds to the Permian–Triassic extinction event (Fig. 6). At the base of the Feixianguan Formation (bed 28), the dominant

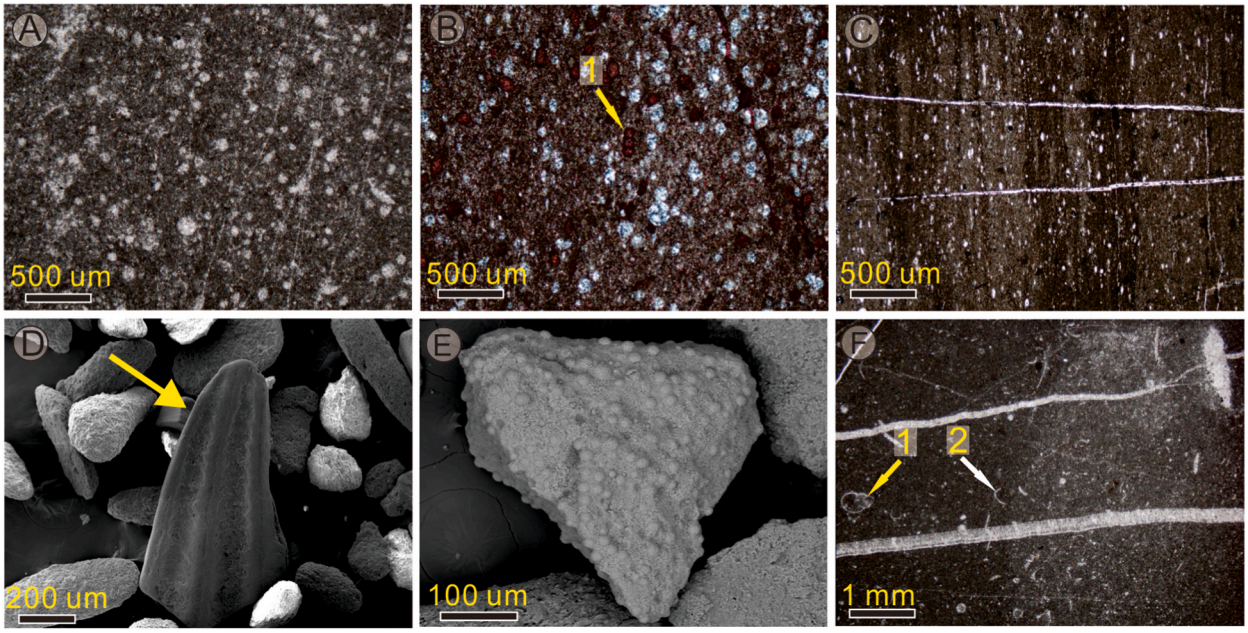

Fig. 7. Microphotographs (A–C, F) and SEM images (D, E) from the Upper Permian–Lower Triassic succession at the Shangsi section. A (bed 22), Radiolarian chert; B (bed 24), Radiolarian chert, 1 = foraminifera; C (bed 26), Radiolarian chert; D (bed 27a), Fragments of the Permian conodont fossils (yellow arrow); E (bed 27c), Microspheres; F (bed 28), Micrite, 1 = gastropods, 2 = bioclasts.

lithologies are gray mudstones, muddy-limestones, and tuffs, with small gastropods and bivalve fossils present. Bed 28 marks the transition to the overlying Feixianguan Formation, characterized by light gray micrites, muddy-limestones, and mudstones, with a few bivalve and gastropod fossils (Fig. 7F).

4.2.2. Wavelet analysis and Fischer plot

After applying the Daubechies wavelet transform to the original gamma-ray data, 50 high-frequency sedimentary cycles have been identified from the top of the Wujiaping Formation to the base of the Feixianguan Formation (Fig. 6). By calculating the difference between the thickness of each cycle and the average thickness of all cycles, as well as the cumulative deviation thickness values, a curve can be plotted using 50 cycle numbers as the x-axis and cumulative deviation thickness values as the y-axis. This curve represents the changing trend of accommodation in the Shangsi section during the Late Permian to Early Triassic, which is roughly equivalent to the relative sea level changes during that period (Fig. 8). Owing to the predominance of carbonate rocks in the lithology, no compaction correction has been applied to the thickness measurements during plotting.

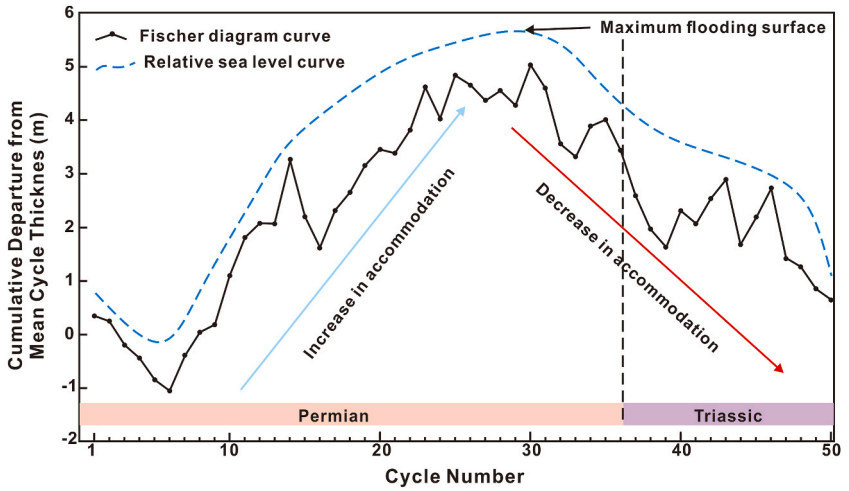

Fig. 8. Fischer plots illustrating the relative sea level curve of the Shangsi section. From the Late Permian to the latest Permian, an increase in accommodation indicates a sea level rise; from the latest Permian to the earliest Triassic, an increase in accommodation indicates a sea level fall.

5. Discussion

5.1. Sedimentary response to sea level fall in the upper Yangtze region during the latest Permian

5.1.1. Sea level fall at Shangsi and Beifengjing

Paleosols, nodules, paleokarsts, and breccias are the products of long-term weathering and dissolution of carbonate rocks after exposure. In addition, they are also important indicators of sea level fall [83]. At the Shangsi section, we did not find sedimentary records indicating a relative sea level fall during the Permian–Triassic transition. However, the approximate left-right symmetry of the Shangsi section can be seen from its Fischer plots (Fig. 8), which indicates that from the latest Permian to the earliest Triassic, the accommodating increased and then decreased, and the corresponding relative sea level increased and then decreased, with the maximum sea flooding surface occurring at cycle number 30.That is, the relative sea level in the Shangsi area began to fall from the latest Permian and continued until the earliest Triassic.

In the Beifengjing section, two paleo-exposure events were identified just below the Permian –Triassic lithostratigraphic boundary (Fig. 9). The first paleo-exposure event occurs at the top of bed 1, exhibiting wave-like undulating structures formed by erosion. It is covered by thick-bedded paleosols of approximately 0.3 m in thickness (Fig. 9A). Under microscopic examination, the original components are observed to have undergone dissolution and were subsequently filled with dark organic matter (Fig. 9C) and coarse-crystalline calcite (Fig. 9D). The second paleo-exposure event is observed in bed 2, characterized by evident paleokarst features (Fig. 9B). The eroded portions were filled with paleosols of approximately 0.5 m in thickness (Fig. 9B), and microscopic analysis reveals original components dissolved and were later filled with dark organic matter, along with residual structures that were not dissolved (Fig. 9E).

Based on the Chongqing Beifengjing section, at the top of the thick bedded bioclastic limestone (bed 1), the presence of *Clarkina changxingensis* and *Clarkina* sp. *indeterminate* allows the determination of the first sea level fall occurring during the latest Permian. For the second paleo-exposure event, although conodont data are lacking, representative latest Permian biota such as *Palaeofusulina* and *Colaniella* are observed in the residual bioclastic limestone formed because of paleokarst. Moreover, no latest Permian fossils are found in the overlying strata, indicating that this sea level fall also occurred during the latest Permian. Therefore, it is concluded that there were two relative sea level falls in the Chongqing Beifengjing area during the latest Permian.

5.1.2. Sea level fall in the Yangtze region

In recent years, multiple sections in the Upper Yangtze region and other areas of South China have reported evidence of sea level fall during the latest Permian. These sections (Fig. 1B) include Longdong, Beibei [62], Jianshuigou, Huayingshan [61], Xiushui [84], Jiangya, Cili [85], Ziyun [60], Moyang [86], and Dawen, Luodian [87]. These sections provide clear sedimentological and paleontological evidence of sea level fall, such as erosion surfaces, paleo-exposure surfaces, and sedimentary hiatuses. Based on the conodont data provided by some of these sections, the timing of sea level fall during the latest Permian varies across different regions, likely

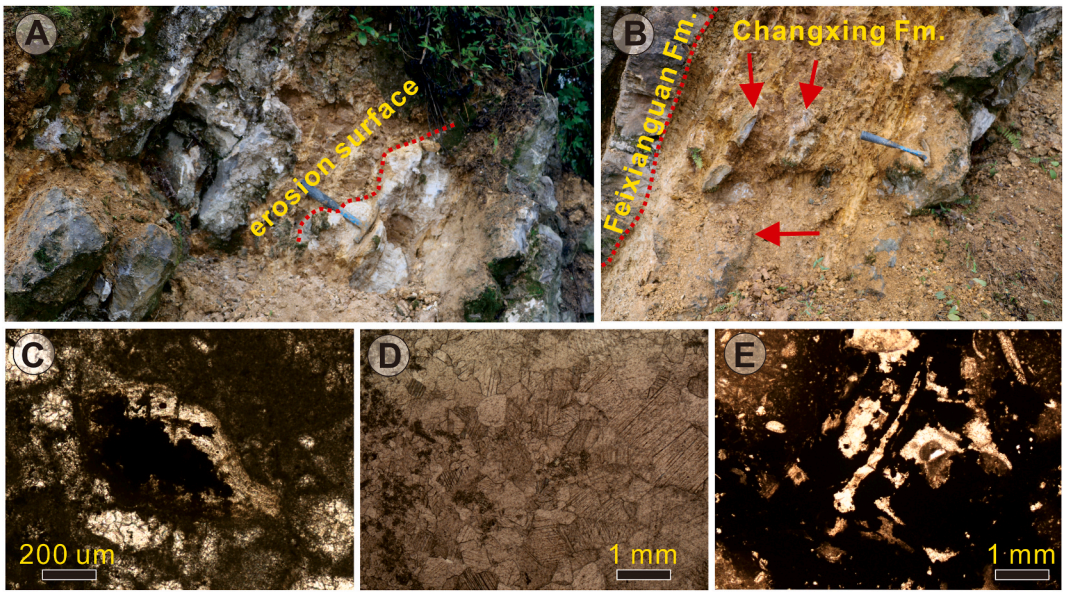

Fig. 9. Macroscopic and microscopic characteristics of the paleo-exposure events in the Beifengjing section. A (bed 1), First paleo-exposure event, erosion surface exhibits a wavy and undulating pattern (red dotted line), overlain by paleosols; B (bed 2), Second paleo-exposure event, visible undissolved residual bioclastic limestone (red arrow) in paleosols; C (bed 1), Original components have undergone dissolution and subsequently filled with dark organic matter. D (bed 1), Original components have undergone dissolution and subsequently filled with coarse-crystalline calcite. E (bed 2), Original components dissolved and were later filled with dark organic matter, along with residual structures that were not dissolved.

because of regional paleogeographic differences [84].

According to the study conducted by Luo et al. on drilling cores in the southern part of the Sichuan Basin, paleokarst development occurred in the Changxing Formation, resulting in a paleokarst unconformity at the top of the Changxing Formation [88]. The key factor leading to the formation of the paleokarst in the Changxing Formation in this area was long-term exposure and dissolution caused by a significant sea level regression during the latest Permian. According to Wu et al., the research on the Changxing Formation reefs in the Beibei area (approximately 10 km from Beifengjing) revealed the presence of at least two paleo-exposure surfaces with karstification at a level equivalent to the Beifengjing section [89]. The first paleo-exposure surface is located at the boundary between the reef cap and the overlying strata, whereas the other one is situated at the top of the reef, just above the boundary with the Lower Triassic Feixianguan Formation. On the top surface of the reef cap, there are karst caves with a depth of approximately 1 m, which are filled with light yellowish-green paleosols [89]. Similarly, Zhou et al. discovered three ancient exposure surfaces near the boundary in the Jiandishuigou section of Huayingshan. The identifying features of these surfaces are ancient karstification, weathered residual paleosol beds, and ferruginous residual limestone beds [61]. Based on the first appearance of the conodont species *Hindeodus parvus*, the first paleo-exposure surface is believed to have occurred during the Late Changxingian, whereas the next two occurred during the Early Griesbachian [61]. When studying the Dawen section in Luodian, Guizhou, Liu et al. found a relative sea level fall event in the *Isarcicella staeschei* Zone to the *I. isarcica* Zone [87]. After that, the sea level began to rise rapidly. The section exhibits sedimentary hiatus, with at least equivalent beds missing from the 24e to 27b beds of the Meishan section (GSSP of PTB at Meishan, Zhejiang) [87].

The research conducted by Wu et al. on the Early Triassic microbialites in Laolongdong section of Beibei, Chongqing, revealed the presence of two sea level fall events near the boundary [62]. The first regression occurred approximately 0.4 m below the PTB and was associated with wave-like erosional surfaces. The second regression appeared approximately 0.4 m above the PTB and exhibited a greater degree of erosion, forming irregular erosional surfaces with height differences of up to 0.3 m. Furthermore, Wu et al. also studied the Jiangxi Xiushui and Guizhou Ziyun sections, and their results indicated the presence of two sea level fall events near the PTB [84]. However, the corresponding sea level fall events occurred at different positions compared with the Laolongdong section. In the Ziyun section, the two regression events occurred at depths of approximately 1.7–2.4 m below the PTB and at the bottom of the *Hindeodus parvus* Zone. In the Xiushui section, both sea level fall occurred below the PTB, with the first one at a depth of 3.1 m below the PTB and the second one at approximately 1.1 m below the PTB. According to Zheng et al., their study on the sedimentary environment near the PTB at the Cili Jiangya section in Hunan province indicated a rapid and substantial relative sea level fall at the uppermost part of the Dalong Formation [85]. Subsequently, from the base of the Daye Formation upward, the relative sea level gradually rose, signifying a transition in the sedimentary environment from a deep-water basin to a shallow-water carbonate platform [85]. In summary, although evidence of sea level fall has been found near the PTB in multiple sections in South China, the number and levels of sea level fall events vary among different sections. Wu et al. explained this phenomenon as a result of sea level fall occurring at different times in different sedimentary environments [84]. The timing differences are likely influenced by variations in ancient topography, where higher elevations experience sea level fall events earlier than lower areas. Modern monitoring data on sea level changes also show significant regional differences, such as faster sea level rise in the mid-Atlantic region compared with the North Atlantic and Maine Bay [90].

Yin et al. conducted a comprehensive study of biostratigraphy and sea level changes in over 20 sections across South China. They concluded that a widespread regression occurred at the end of the Permian in the entire South China region, leading to sedimentary hiatuses on shallow-water carbonate platforms in the Hunan–Guizhou–Guangxi basin. The lowest sea level was determined to be around the time of the *Clarkina meishanensis* and *Hindeodus changxingensis* Zones, which is well correlated with the main episode of the EPME [65].

Based on the research conducted on the Shangsi and Beifengjing sections in this study, along with previous research findings, it can be concluded that there was a relative sea level fall during the latest Permian in the Upper Yangtze region and even in the South China region. Furthermore, this sea level fall persisted until the earliest Triassic.

5.2. Implications of the latest Permian regression for mass extinctions

Reviewing the five major and several smaller biological extinction events during geologic history, it is easy to see that most of the biological event extinctions coincide highly in time with sea level rise and fall turning points. That is, almost all mass species extinctions are associated with rapid fluctuations in sea level on a global scale [52]. Slow changes in sea level may have a negligible effect on organisms, but rapid and large sea level falls or rises may result in the turnover or even extinction of some species of organisms [52,53].

Although extensive regression events occurred in the Upper Yangzi region, as well as in other parts of South China at the latest Permian, the relationship between sea level fall and biological extinction requires further discussion. The argument that sea level fall leads to extinctions is based on the massive loss of shallow marine habitats [91], which is disputed by Erwin [53], who argues that the species-area effect cannot be directly applied to past geohistoric periods and marine environments. He also points out that the species-area effect focuses more on the regional diversity of habitats within a region rather than on the absolute size of the habitat. In a similar vein, explanations of the first phase of the late Ordovician extinction have tended to focus on the rapid global cooling as the primary cause of the extinction rather than emphasizing the reduction in the area of shallow marine shelters [92]. The biotic extinction event at the end-Guadalupian may, to some extent, be related to a significant sea level regression [93,94]. However, the environmental impact of contemporaneous volcanic activity in the Emeishan Large Igneous Province cannot be underestimated [95,96].

Based on the evidence from the Chongqing Beifengjing section regarding the two sea level regressions and biotic abundance, it can be observed that after the first sea level regression, there was not a significant change in biotic abundance. After the second sea level

regression, representative Permian organisms such as fusulinids completely disappeared, and only a very small amount of biotic fossils were found in the lowermost part of the Feixianguan Formation. Therefore, solely relying on the reduction in shallow marine habitat caused by sea level fall appears insufficient to explain the EPME. This is because the inferred difference in sea level regression magnitudes based on the thickness of paleosol beds filled in the strata is very small. However, the first sea level regression did not cause mass extinction, but likely impacted some species (e.g., *Colaniella*, *Codonofusiella*). Furthermore, during the Late Guadalupian, there was a globally significant and substantial sea level fall, lowering sea levels to their lowest position during the Phanerozoic era [97,98]. However, the largest mass extinction event in geological history occurred at the latest Permian, not during the Late Guadalupian.

Examining the Shangsi section, the relative sea level regression event spans across the PTB and continues until the earliest Triassic. There are multiple tuff beds (beds 22 to 28) in the P-T strata (Fig. 6), which have been proven to have a volcanic origin [57,99–101]. This indicates that there were at least several episodes of volcanic activity during the regression period. In the Beifengjing section, a tuffaceous bed with a thickness of approximately 7 cm was deposited at the top of the Changxing Formation (bed 3), indicating that the Beifengjing area was also influenced by volcanic activity. Similarly, in the Upper Yangtze region and other parts of South China, volcanic tuff beds are also present near the PTB in multiple sections, suggesting that South China was widely affected by volcanic activity during the latest Permian. Volcanic activity and frequent wildfires [102] accelerate the input of terrigenous debris into the ocean, leading to the deterioration of the marine environment (e.g., soil-induced turbidity, eutrophication and anoxia) [103,104]. After studying six PTB sections in southern China, Tian et al. concluded that enhanced terrestrial input, anomalous ocean circulation, and various geochemical processes led to fluctuations in carbonate saturation, which were sedimentary responses to volcanic eruptions [105]. In three sections of the Nanpanjiang Basin, a “foram gap” and concurrent “detrital events” are observed, occurring before the EPME. This reflects the instability of marine environments on the eve of the EPME [106].

Based on the analysis above, a model is hypothesized to explain the EPME, suggesting that there was a sea regression and frequent volcanic activity during the latest Permian, resulting in extensive exposure of shallow ocean areas. This led to the deterioration of marine environments due to the influx of terrigenous debris, increasing the survival pressure on marine organisms. Because the occurrence of the EPME is complex, other factors driving the EPME cannot be ruled out.

6. Conclusions

We used sedimentology, wavelet analysis, and Fischer plots to analyze the relative sea level changes in the Shangsi and Beifengjing sections. We discussed their implications on the EPME and derived the following key conclusions.

(1) During the latest Permian, there was a sea level fall in the Yangtze region. In the Beifengjing section, located in a carbonate platform sedimentary environment, two paleo-exposure surfaces were observed at the top of the Changxing Formation. These surfaces exhibit karstification and are filled with paleosols, representing two episodes of relative sea level fall. In the Shangsi section, situated in a relatively deep-water sedimentary environment, the Fischer plot analysis also indicates that the relative sea level began to fall at the latest Permian and continued until the earliest Triassic.
(2) The reduction of shallow marine habitat caused by sea level fall cannot cause mass extinctions. However, sea level fall can increase the input of terrestrial debris into the ocean, leading to the deterioration of the marine environment. During the sea level fall period, the South China region experienced frequent volcanic eruptions. The combined adverse effects of volcanic eruptions, sea level fall, and other events exceeded the threshold for biological survival, resulting in the catastrophic EPME.

Funding

This study was supported by NSF grants (No. 41572085) of the Chinese Ministry of Science and Technology, the Natural Science Foundation of Sichuan Province (2022NSFSC1177) and the Fundamental Research Funds of China West Normal University (20E031).

Data availability statement

The data that support the findings of this study are openly available in Science Data Bank at https://doi.org/10.57760/sciencedb.08197.

CRediT authorship contribution statement

Xiong Duan: Writing – original draft, Methodology, Investigation, Funding acquisition. **Zhiqiang Shi:** Writing – review & editing, Project administration, Funding acquisition.

Declaration of competing interest

The authors declare that they have no known competing financial interests or personal relationships that could have appeared to influence the work reported in this paper.

References

[1] P.B. Wignall, A. Hallam, Anoxia as a cause of the Permian/Triassic mass extinction: facies evidence from northern Italy and the western United States, Palaeogeogr. Palaeoclimatol. Palaeoecol. 93 (1992) 21–46, https://doi.org/10.1016/0031-0182(92)90182-5.
[2] D.H. Erwin, The permo–triassic extinction, Nature 367 (1994) 231–236, https://doi.org/10.1038/367231a0.
[3] S.M. Stanley, Estimates of the magnitudes of major marine mass extinctions in earth history, Proc. Natl. Acad. Sci. USA 113 (2016) E6325–E6334, https://doi.org/10.1073/pnas.161309411.
[4] P.M. Rees, Land-plant diversity and the end-Permian mass extinction, Geology 30 (2002) 827–830, https://doi.org/10.1130/0091-7613(2002)030<0827:LPDATE>2.0.CO;2.
[5] B. Cascales-Miñana, J.B. Diez, P. Gerrienne, C.J. Cleal, A palaeobotanical perspective on the great end-Permian biotic crisis, Hist. Biol. 28 (2016) 1066–1074, https://doi.org/10.1080/08912963.2015.1103237.
[6] H. Nowak, E. Schneebeli-Hermann, E. Kustatscher, No mass extinction for land plants at the Permian–Triassic transition, Nat. Commun. 10 (2019) 1–8, https://doi.org/10.1038/s41467-018-07945-w.
[7] Z.-Q. Chen, T.J. Algeo, D.J. Bottjer, Global review of the Permian–Triassic mass extinction and subsequent recovery: Part I, Earth Sci. Rev. 137 (2014) 1–5, https://doi.org/10.1016/j.earscirev.2014.05.007.
[8] T.J. Algeo, Z.-Q. Chen, D.J. Bottjer, Global review of the Permian–Triassic mass extinction and subsequent recovery: Part II, Earth Sci. Rev. 149 (2015) 1–4, https://doi.org/10.1016/j.earscirev.2015.09.007.
[9] R.E. Ernst, N. Youbi, How Large Igneous Provinces affect global climate, sometimes cause mass extinctions, and represent natural markers in the geological record, Palaeogeogr. Palaeoclimatol. Palaeoecol. 478 (2017) 30–52, https://doi.org/10.1016/j.palaeo.2017.03.014.
[10] Y. Isozaki, Superanoxia across the Permo-Triassic boundary: record in accreted deep-sea pelagic chert in Japan, Pangea: global environments and resources & Canad, Soc.Petrol.Geol.Mem 17 (1994) 805–812, https://doi.org/10.5575/geosoc.100.XIX.
[11] P.B. Wignall, R.J. Twitchett, Oceanic anoxia and the end permian mass extinction, Science 272 (1996) 1155–1158, https://doi.org/10.1126/science.272.5265.1155.
[12] Y. Isozaki, Permo-triassic boundary superanoxia and stratified superocean: records from lost deep sea, Science 276 (1997) 235–238, https://doi.org/10.1126/science.276.5310.2.
[13] K. Grice, C. Cao, G.D. Love, M.E. Böttcher, R.J. Twitchett, E. Grosjean, R.E. Summons, S.C. Turgeon, W. Dunning, Y. Jin, Photic zone euxinia during the permian-triassic superanoxic event, Science 307 (2005) 706–709, https://doi.org/10.1126/science.1104323.
[14] Y. Wang, J. Tong, J. Wang, X. Zhou, Calcimicrobialite after end-Permian mass extinction in South China and its palaeoenvironmental significance, Chin. Sci. Bull. 50 (2005) 665–671, https://doi.org/10.1360/982004-323.
[15] D.P.G. Bond, P.B. Wignall, Pyrite framboid study of marine Permian–Triassic boundary sections: a complex anoxic event and its relationship to contemporaneous mass extinction, GSA Bulletin 122 (2010) 1265–1279, https://doi.org/10.1130/B30042.1.
[16] J. Shen, Q. Feng, T.J. Algeo, C. Li, N.J. Planavsky, L. Zhou, M. Zhang, Two pulses of oceanic environmental disturbance during the Permian–Triassic boundary crisis, Earth Planet Sci. Lett. 443 (2016) 139–152, https://doi.org/10.1016/j.epsl.2016.03.030.
[17] L. Wang, P.B. Wignall, Y. Wang, H. Jiang, Y. Sun, G. Li, J. Yuan, X. Lai, Depositional conditions and revised age of the permo-triassic microbialites at gaohua section, Cili county (hunan province, South China), Palaeogeogr. Palaeoclimatol. Palaeoecol. 443 (2016) 156–166, https://doi.org/10.1016/j.palaeo.2015.11.032.
[18] M.J. Benton, R.J. Twitchett, How to kill (almost) all life: the end-Permian extinction event, Trends Ecol. Evol. 18 (2003) 358–365, https://doi.org/10.1016/S0169-5347(03)00093-4.
[19] Y. Sun, M.M. Joachimski, P.B. Wignall, C. Yan, Y. Chen, H. Jiang, L. Wang, X. Lai, Lethally hot temperatures during the early triassic greenhouse, Science 338 (2012) 366–370, https://doi.org/10.1126/science.1224126.
[20] Y. Cui, Climate swings in extinction, Nat. Geosci. 11 (2018) 889–890, https://doi.org/10.1038/s41561-018-0264-8.
[21] Y. Cui, L.R. Kump, A. Ridgwell, Initial assessment of the carbon emission rate and climatic consequences during the end-Permian mass extinction, Palaeogeogr. Palaeoclimatol. Palaeoecol. 389 (2013) 128–136, https://doi.org/10.1016/j.palaeo.2013.09.001.
[22] M.M. Joachimski, X. Lai, S. Shen, H. Jiang, G. Luo, B. Chen, J. Chen, Y. Sun, Climate warming in the latest Permian and the Permian–Triassic mass extinction, Geology 40 (2012) 195–198, https://doi.org/10.1130/G32707.1.
[23] H. Svensen, S. Planke, A.G. Polozov, N. Schmidbauer, F. Corfu, Y.Y. Podladchikov, B. Jamtveit, Siberian gas venting and the end-Permian environmental crisis, Earth Planet Sci. Lett. 277 (2009) 490–500, https://doi.org/10.1016/j.epsl.2008.11.015.
[24] B.A. Black, J.-F. Lamarque, C.A. Shields, L.T. Elkins-Tanton, J.T. Kiehl, Acid rain and ozone depletion from pulsed Siberian Traps magmatism, Geology 42 (2014) 67–70, https://doi.org/10.1130/G34875.1.
[25] J.P. Benca, I.A.P. Duijnstee, C.V. Looy, UV-B–induced forest sterility: implications of ozone shield failure in Earth's largest extinction, Sci. Adv. 4 (2018) e1700618, https://doi.org/10.1126/sciadv.1700618.
[26] M.W. Broadley, P.H. Barry, C.J. Ballentine, L.A. Taylor, R. Burgess, End-Permian extinction amplified by plume-induced release of recycled lithospheric volatiles, Nat. Geosci. 11 (2018) 682–687, https://doi.org/10.1038/s41561-018-0215-4.
[27] A. Montenegro, P. Spence, K.J. Meissner, M. Eby, M.J. Melchin, S.T. Johnston, Climate simulations of the Permian-Triassic boundary: ocean acidification and the extinction event, Paleoceanography 26 (2011) PA3207, https://doi.org/10.1029/2010PA002058.
[28] J.L. Hinojosa, S.T. Brown, J. Chen, D.J. DePaolo, A. Paytan, S.-z. Shen, J.L. Payne, Evidence for end-Permian ocean acidification from calcium isotopes in biogenic apatite, Geology 40 (2012) 743–746, https://doi.org/10.1130/G33048.1.
[29] E. Heydari, N. Arzani, M. Safaei, J. Hassanzadeh, Ocean's response to a changing climate: clues from variations in carbonate mineralogy across the Permian–Triassic boundary of the Shareza Section, Iran, Global Planet. Change 105 (2013) 79–90, https://doi.org/10.1016/j.gloplacha.2012.12.013.
[30] M.O. Clarkson, S.A. Kasemann, R.A. Wood, T.M. Lenton, S.J. Daines, S. Richoz, F. Ohnemueller, A. Meixner, S.W. Poulton, E.T. Tipper, Ocean acidification and the Permo-Triassic mass extinction, Science 348 (2015) 229–232, https://doi.org/10.1126/science.aaa0191.
[31] H. Sanei, S.E. Grasby, B. Beauchamp, Latest Permian mercury anomalies, Geology 40 (2012) 63–66, https://doi.org/10.1130/G32596.1.
[32] S.E. Grasby, B. Beauchamp, D.P.G. Bond, P. Wignall, C. Talavera, J.M. Galloway, K. Piepjohn, L. Reinhardt, D. Blomeier, Progressive environmental deterioration in northwestern Pangea leading to the latest Permian extinction, GSA Bulletin 127 (2015) 1331–1347, https://doi.org/10.1130/B31197.1.
[33] S.E. Grasby, B. Beauchamp, D.P.G. Bond, P.B. Wignall, H. Sanei, Mercury anomalies associated with three extinction events (capitanian crisis, latest permian extinction and the smithian/spathian extinction) in NW pangea, Geol. Mag. 153 (2016) 285–297, https://doi.org/10.1017/S0016756815000436.
[34] X. Wang, P.A. Cawood, H. Zhao, L. Zhao, S.E. Grasby, Z.-Q. Chen, L. Zhang, Global mercury cycle during the end-Permian mass extinction and subsequent Early Triassic recovery, Earth Planet Sci. Lett. 513 (2019) 144–155, https://doi.org/10.1016/j.epsl.2019.02.026.
[35] J. Shen, J. Chen, T.J. Algeo, S. Yuan, Q. Feng, J. Yu, L. Zhou, B. O'Connell, N.J. Planavsky, Evidence for a prolonged Permian–Triassic extinction interval from global marine mercury records, Nat. Commun. 10 (2019) 1563, https://doi.org/10.1038/s41467-019-09620-0.
[36] L. Becker, R.J. Poreda, A.G. Hunt, T.E. Bunch, M. Rampino, Impact event at the permian-triassic boundary: evidence from extraterrestrial noble gases in fullerenes, Science 291 (2001) 1530–1533, https://doi.org/10.1126/science.1057243.
[37] L. Becker, R.J. Poreda, A.R. Basu, K.O. Pope, T.M. Harrison, C. Nicholson, R. Iasky, Bedout: a possible end-permian impact crater offshore of northwestern Australia, Science 304 (2004) 1469–1476, https://doi.org/10.1126/science.1093925.
[38] K. Kaiho, Y. Kajiwara, T. Nakano, Y. Miura, H. Kawahata, K. Tazaki, M. Ueshima, Z. Chen, G.R. Shi, End-Permian catastrophe by a bolide impact: evidence of a gigantic release of sulfur from the mantle, Geology 29 (2001) 815–818, https://doi.org/10.1130/0091-7613(2001)029<0815:EPCBAB>2.0.CO, 2.
[39] C. Koeberl, K.A. Farley, B. Peucker-Ehrenbrink, M.A. Sephton, Geochemistry of the end-Permian extinction event in Austria and Italy: No evidence for an extraterrestrial component, Geology 32 (2004) 1053–1056, https://doi.org/10.1130/G20907.1.

[40] H. Zhang, S.-z. Shen, C.-q. Cao, Q.-f. Zheng, Origins of microspherules from the Permian–Triassic boundary event layers in South China, Lithos 204 (2014) 246–257, https://doi.org/10.1016/j.lithos.2014.02.018.
[41] P.B. Wignall, Large igneous provinces and mass extinctions, Earth Sci. Rev. 53 (2001) 1–33, https://doi.org/10.1016/S0012-8252(00)00037-4.
[42] V.E. Courtillot, P.R. Renne, On the ages of flood basalt events, Compt. Rendus Geosci. 335 (2003) 113–140, https://doi.org/10.1016/S1631-0713(03)00006-3.
[43] M.K. Reichow, M.S. Pringle, A.I. Al'Mukhamedov, M.B. Allen, V.L. Andreichev, M.M. Buslov, C.E. Davies, G.S. Fedoseev, J.G. Fitton, S. Inger, A.Y. Medvedev, C. Mitchell, V.N. Puchkov, I.Y. Safonova, R.A. Scott, A.D. Saunders, The timing and extent of the eruption of the Siberian Traps large igneous province: implications for the end-Permian environmental crisis, Earth Planet Sci. Lett. 277 (2009) 9–20, https://doi.org/10.1016/j.epsl.2008.09.030.
[44] D.L. Kidder, T.R. Worsley, Phanerozoic large igneous provinces (LIPs), HEATT (haline euxinic acidic thermal transgression) episodes, and mass extinctions, Palaeogeogr. Palaeoclimatol. Palaeoecol. 295 (2010) 162–191, https://doi.org/10.1016/j.palaeo.2010.05.036.
[45] D.P.G. Bond, P.B. Wignall, Large igneous provinces and mass extinctions: an update, in: G. Keller, A.C. Kerr (Eds.), Volcanism, Impacts, and Mass Extinctions: Causes and Effects, 2014, pp. 29–55, https://doi.org/10.1130/2014.2505(02. Geological Society of America.
[46] D.P.G. Bond, S.E. Grasby, On the causes of mass extinctions, Palaeogeogr. Palaeoclimatol. Palaeoecol. 478 (2017) 3–29, https://doi.org/10.1016/j.palaeo.2016.11.005.
[47] W. Holser, M. Magaritz, Events near the permian–triassic boundary, Mod. Geol. 11 (1987) 155–180, https://doi.org/10.1016/0016-7037(92)90306-4.
[48] T.J.M. Schopf, Permo-triassic extinctions: relation to sea-floor spreading, J. Geol. 82 (1974) 129–143, https://doi.org/10.1086/627955.
[49] D.S. Simberloff, Permo-triassic extinctions: effects of area on biotic equilibrium, J. Geol. 82 (1974) 267–274, https://doi.org/10.1086/627962.
[50] J.W. Valentine, E.M. Moores, Plate-Tectonic regulation of faunal diversity and sea level: a model, Nature 228 (1970) 657–659, https://doi.org/10.1038/228657a0.
[51] A. Hallam, J.M. Cohen, The case for sea-level change as a dominant causal factor in mass extinction of marine invertebrates [and discussion], Philosophical Transactions of the Royal Society of London. Series B, Biological Sciences 325 (1989) 437–455, https://doi.org/10.1098/rstb.1989.0098.
[52] A. Hallam, P.B. Wignall, Mass extinctions and sea-level changes, Earth Sci. Rev. 48 (1999) 217–250, https://doi.org/10.1016/S0012-8252(99)00055-0.
[53] D.H. Erwin, The Great Paleozoic Crisis: Life and Death in the Permian, Columbia University Press, New York, 1993.
[54] C.A. Ross, J.R.P. Ross, Late Paleozoic sea levels and depositional sequences, Geology Faculty Publications 24 (1987) 137–149.
[55] B.U. Haq, J. Hardenbol, P.R. Vail, L.E. Stover, J.P. Colin, N.S. Ioannides, R.C. Wright, G.R. Baum, A.M. Gombos Jr., C.E. Pflum, T.S. Loutit, R.J.d. Chêne, K. K. Romine, J.F. Sarg, H.W. Posamentier, B.E. Morgan, Mesozoic and cenozoic chronostratigraphy and cycles of sea-level change, in: C.K. Wilgus, B.S. Hastings, H. Posamentier, J.V. Wagoner, C.A. Ross, C.G.S.C. Kendall (Eds.), Sea-Level Changes: an Integrated Approach, SEPM Society for Sedimentary Geology, 1988, pp. 71–108, https://doi.org/10.2110/pec.88.01.0071.
[56] Z. Chen, The late permian global flooding events, Sediment. Facies Palaeogeogr. 15 (1995) 34–39 (in Chinese with English abstract).
[57] Z. Yang, S. Wu, Geological Events of Permo-Triassic Transitional Period in South China, Geological Publishing House, Beijing, 1991 (in Chinese with English abstract).
[58] P.B. Wignall, A. Hallam, Griesbachian (Earliest Triassic) palaeoenvironmental changes in the Salt Range, Pakistan and southeast China and their bearing on the Permo-Triassic mass extinction, Palaeogeogr. Palaeoclimatol. Palaeoecol. 102 (1993) 215–237, https://doi.org/10.1016/0031-0182(93)90068-T.
[59] H. Yin, Advancements of permian and triassic research, Adv. Earth Sci. 9 (1994) 1–10 (in Chinese with English abstract).
[60] Y. Wu, J. Fan, Y. Jin, Emergence of the late permian changhsingian reefs at the end of the permian, Acta Geol. Sin. 77 (2003) 289–298 (in Chinese with English abstract).
[61] G. Zhou, R.C. Zheng, P. Luo, C. Zheng, J.L. Cai, H. Wen, Geological events and their geochemical responses of the permian-triassic boundary, huaying, eastern sichuan, Earth Sci. J. China Univ. Geosci. 37 (2012) 101–110 (in Chinese with English abstract).
[62] Y.S. Wu, H. Jiang, T. Liao, Sea-Level drops in the permian-triassic boundary section at Laolongdong, chongqing, sichuan province, Acta Petrol. Sin. 22 (2006) 2405–2415 (in Chinese with English abstract).
[63] P.B. Wignall, A. Hallam, Facies change and the end-permian mass extinction in S.E. Sichuan, China, Palaios 11 (1996) 587–596, https://doi.org/10.2307/3515193.
[64] S. Wu, Z.-Q. Chen, Y. Fang, Y. Pei, H. Yang, J. Ogg, A Permian-Triassic boundary microbialite deposit from the eastern Yangtze Platform (Jiangxi Province, South China): geobiologic features, ecosystem composition and redox conditions, Palaeogeogr. Palaeoclimatol. Palaeoecol. 486 (2017) 58–73, https://doi.org/10.1016/j.palaeo.2017.05.015.
[65] H. Yin, H. Jiang, W. Xia, Q. Feng, N. Zhang, J. Shen, The end-Permian regression in South China and its implication on mass extinction, Earth Sci. Rev. 137 (2014) 19–33, https://doi.org/10.1016/j.earscirev.2013.06.003.
[66] Z. Luo, Y. Jin, X. Zhao, The emei Taphrogenesis of the upper Yangtze platform in SouthSouth China, Geol. Mag. 127 (1990) 393–405 (in Chinese with English abstract).
[67] Y. Wang, Y. Wen, H. Hong, M. Xia, Y. Fan, L. Wen, L. Kong, C. Wu, Carbonate slope facies sedmentary characteristics of the late pemian to early triassic in northern Sichuan Basin, J. Palaeogeogr. 11 (2009) 143–156 (in Chinese with English abstract).
[68] Z. Feng, Y. Yang, Z. Jin, Y. He, S. Wu, W. Xin, Z. Bao, J. Tan, Lithofacies paleogeography of the permian of SouthSouth China, Acta Sedimentol. Sin. 14 (1996) 1–11 (in Chinese with English abstract).
[69] Y. Zhu, H. Luo, H.-W. Cai, X.U. Bo, H. Yang, Y. Zhao, D. Chen, Stratigraphic division of the early and middle triassic at the xiejiacao section in guang'an, sichuan, J. Stratigr. 36 (2012) 784–791 (in Chinese with English abstract).
[70] K. Huang, S. Huang, Z. Hu, Y. Zhong, X. Li, Carbon isotopic composition and evolution of the lower triassic marine carbonates from dukou of xuanhan and Beibei of chongqing, J. Palaeogeogr. 18 (2016) 101–114 (in Chinese with English abstract).
[71] T.J. Algeo, C.M. Henderson, J. Tong, Q. Feng, H. Yin, R.V. Tyson, Plankton and productivity during the Permian–Triassic boundary crisis: an analysis of organic carbon fluxes, Global Planet. Change 105 (2013) 52–67, https://doi.org/10.1016/j.gloplacha.2012.02.008.
[72] Z. Feng, Z. Bao, S. Wu, Y. Li, G. Wang, Lithofacies Palaeogeography of Early and Middle Triassic of South China, Petroleum Industry Press, Beijing, 1997 (in Chinese with English abstract).
[73] Q. Li, S. Yang, K. Azmy, H. Chen, M. Hou, Z. Wang, S. Xu, D. Yang, X. Zhang, A. Chen, Strontium isotope evolution of middle permian seawater in the Sichuan Basin, South China: possible causes and implications, Palaeogeogr. Palaeoclimatol. Palaeoecol. 565 (2021) 110188, https://doi.org/10.1016/j.palaeo.2020.110188.
[74] Z. Li, L. Zhan, X. Zhu, J. Zhang, R. Jun, G. Liu, H. Sheng, G. Shen, J. Dai, H. Huang, L. Xie, Z. Yan, J. Yao, Mass extinction and geological events between Palaeozoic and Mesozoic era, Acta Geol. Sin. 60 (1986) 1–15 (in Chinese with English abstract).
[75] J.H. Zhang, J.Y. Dai, S.G. Tian, Biostratigraphy of late permian and early triassic conodonts in Shangsi, guangyuan county, sichuan, China, in: Scientific Papers on Geology for International Exchange–Prepared for the 27th International Geological Congress, vol. 1, Geological Publishing House, Beijing, 1984 (In Chinese with English abstract).
[76] R. Jin, H. Huang, Sedimentary features and environmental evolution of the permian-triassic boundary section in Shangsi, guangyuan, sichuan province, Prof. Pap. Stratigr. Palaeontol. 18 (1987) 32–75 (In Chinese with English abstract).
[77] P.B. Wignall, R.J. Twitchett, Unusual intraclastic limestones in Lower Triassic carbonates and their bearing on the aftermath of the end-Permian mass extinction, Sedimentology 46 (1999) 303–316, https://doi.org/10.1046/j.1365-3091.1999.00214.x.
[78] Z. Shi, H. Yi, D. Zeng, H. Zhang, The lowest member of lower triassic Feixianguan Formation in upper Yangtze region:sedimentary records from sluggish water to turbulent ocean after the mass extinction, Geol. Rev. 56 (2010) 769–780 (In Chinese with English abstract).
[79] F. Heller, W. Lowrie, L. Huamei, W. Junda, Magnetostratigraphy of the permo-triassic boundary section at Shangsi (guangyuan, sichuan province, China), Earth Planet Sci. Lett. 88 (1988) 348–356, https://doi.org/10.1016/0012-821X(88)90091-X.
[80] H. Jiang, X. Lai, C. Yan, R. Aldridge, P. Wignall, Y. Sun, Revised conodont zonation and conodont evolution across the permian–triassic boundary at the Shangsi section, guangyuan, sichuan, South China, Global Planet. Change 77 (2011) 103–115, https://doi.org/10.1016/j.gloplacha.2011.04.003.

[81] W. Zhao, Z. Jiang, L. Qiu, Y. Chen, Geological concept,method and application of sequence unit identification through wavelet analysis, Oil Gas Geol. 31 (2010) 436–441 (In Chinese with English abstract).
[82] P.M. Sadler, D.A. Osleger, I.P. Montanez, On the labeling, length, and objective basis of Fischer plots, J. Sediment. Res. 63 (1993) 360–368, https://doi.org/10.1306/D4267AFF-2B26-11D7-8648000102C1865D.
[83] L. Guo, X. Xie, H. Chen, Diagenesis related to ancient exposed surfaces in carbonate rocks, Geol. Sci. Technol. Inf. 33 (2014) 57–62 (In Chinese with English abstract).
[84] Y. Wu, W. Yang, H. Jiang, J. Fan, Petrologic evidence for sea-level drop in latest Permian in Jiangxi province, China and its meanings for the mass extinction, Acta Petrol. Sin. 22 (2006) 3039–3046 (In Chinese with English abstract).
[85] Q. Zheng, Y. Ding, C. Cao, Microfacies, sedimentary environment and sea-level changes of the Permian-Triassic boundary succession in the Jiangya section, Cili County, Hunan Province, Acta Petrol. Sin. 29 (2013) 3637–3648 (In Chinese with English abstract).
[86] F. Li, X. Wu, Characteristics and palaeoenvironmental significances of shallow-marine sediments in the latest Permian,Moyang Section,Guizhou, Acta Sedimentol. Sin. 30 (2012) 679–688 (In Chinese with English abstract).
[87] J. Liu, Y. Ezaki, S.R. Yang, H. Wang, N. Adachi, Age and sedimentology of microbialites after the end-Permian mass extinction in Luodian, Guizhou Province, J. Palaeogeogr. 9 (2007) 473–486 (In Chinese with English abstract).
[88] B. Luo, X. Tan, L. Li, H. Liu, J. Xia, B. Du, X. Liu, X. Mou, Discovery and geologic significance of paleokarst unconformity between Changxing Formation and Feixianguan Formation in shunan area of Sichuan Basin, Acta Pet. Sin. 31 (2010) 408–414 (In Chinese with English abstract).
[89] X. Wu, X. Liu, Z. Yang, X. Chen, Formation of reef-bound reservoirs of upper permian changxing Formation in east sichuan, Oil Gas Geol. 11 (1990) 282–297 (In Chinese with English abstract).
[90] C.G. Piecuch, P. Huybers, C.C. Hay, A.C. Kemp, C.M. Little, J.X. Mitrovica, R.M. Ponte, M.P. Tingley, Origin of spatial variation in US East Coast sea-level trends during 1900–2017, Nature 564 (2018) 400–404, https://doi.org/10.1038/s41586-018-0787-6.
[91] N.D. Newell, Revolutions in the history of life, in: C.C. Albritton, Jr (Ed.), Uniformity and Simplicity: A Symposium on the Principle of the Uniformity of Nature, Geological Society of America, 1967, pp. 63–92, https://doi.org/10.1130/SPE89-p63.
[92] R.J. Twitchett, The palaeoclimatology, palaeoecology and palaeoenvironmental analysis of mass extinction events, Palaeogeogr. Palaeoclimatol. Palaeoecol. 232 (2006) 190–213, https://doi.org/10.1016/j.palaeo.2005.05.019.
[93] Z. Qiu, Q. Wang, C. Zou, D. Yan, H. Wei, Transgressive–regressive sequences on the slope of an isolated carbonate platform (Middle–Late Permian, Laibin, South China), Facies 60 (2014) 327–345, https://doi.org/10.1007/s10347-012-0359-4.
[94] D. Kofukuda, Y. Isozaki, H. Igo, A remarkable sea-level drop and relevant biotic responses across the Guadalupian–Lopingian (Permian) boundary in low-latitude mid-Panthalassa: irreversible changes recorded in accreted paleo-atoll limestones in Akasaka and Ishiyama, Japan, J. Asian Earth Sci. 82 (2014) 47–65, https://doi.org/10.1016/j.jseaes.2013.12.010.
[95] Y. Isozaki, Integrated "plume winter" scenario for the double-phased extinction during the Paleozoic–Mesozoic transition: the G-LB and P-TB events from a Panthalassan perspective, J. Asian Earth Sci. 36 (2009) 459–480, https://doi.org/10.1016/j.jseaes.2009.05.006.
[96] P.B. Wignall, Y. Sun, D.P.G. Bond, G. Izon, R.J. Newton, S. Védrine, M. Widdowson, J.R. Ali, X. Lai, H. Jiang, H. Cope, S.H. Bottrell, Volcanism, mass extinction, and carbon isotope fluctuations in the middle permian of China, Science 324 (2009) 1179–1182, https://doi.org/10.1126/science.1171956.
[97] K.G. Miller, M.A. Kominz, J.V. Browning, J.D. Wright, G.S. Mountain, M.E. Katz, P.J. Sugarman, B.S. Cramer, N. Christie-Blick, S.F. Pekar, The phanerozoic record of global sea-level change, Science 310 (2005) 1293–1298, https://doi.org/10.1126/science.1116412.
[98] B.U. Haq, S.R. Schutter, A chronology of paleozoic sea-level changes, Science 322 (2008) 64–68, https://doi.org/10.1126/science.1161648.
[99] H.F. Yin, S.J. Huang, K.X. Zhang, F.J. Yang, M.H. Ding, X.M. Bi, S.X. Zhang, Volcanism al the Permian-Trissic boundary in South China and its effects on mass extinction, Acta Geol. Sin. 2 (1989) 169–180.
[100] Y. Zhou, Z. Chai, X. Mao, S. Ma, J. Ma, Rare earth geochemistry of clays at and near the permian-triassic boundary in SouthSouth China, Geotect. Metallogenia 13 (1989) 188–196 (In Chinese with English abstract).
[101] Y. Gan, L.S. Yu, M.Y. He, Y. Zhang, F. Liu, Y.T. Wang, W. Que, REE geochemistry of claystone at the Permian-Triassic boundary in the Jiangyou-Guangyuan area, northern Sichuan, China and its geological implications, Geol. Bull. China 27 (2008) 380–387 (In Chinese with English abstract).
[102] F. Hua, L. Shao, X. Wang, T.P. Jones, T. Zhang, D.P.G. Bond, Z. Yan, J. Hilton, The impact of frequent wildfires during the Permian–Triassic transition: floral change and terrestrial crisis in southwestern China, Palaeogeogr. Palaeoclimatol. Palaeoecol. 641 (2024) 112129, https://doi.org/10.1016/j.palaeo.2024.112129.
[103] M.A. Sephton, C.V. Looy, H. Brinkhuis, P.B. Wignall, J.W. de Leeuw, H. Visscher, Catastrophic soil erosion during the end-Permian biotic crisis, Geology 33 (2005) 941–944, https://doi.org/10.1130/G21784.1.
[104] X.-T. Xu, L.-Y. Shao, B. Lan, S. Wang, J. Hilton, J.-Y. Qin, H.-H. Hou, J. Zhao, Continental chemical weathering during the early cretaceous oceanic anoxic event (OAE1b): a case study from the fuxin fluvio-lacustrine basin, liaoning province, NE China, J. Palaeogeogr. 9 (2020) 12, https://doi.org/10.1186/s42501-020-00056-y.
[105] L. Tian, J. Tong, D. Bottjer, D. Chu, L. Liang, H. Song, H. Song, Rapid carbonate depositional changes following the Permian-Triassic mass extinction: sedimentary evidence from South China, J. Earth Sci. 26 (2015) 166–180, https://doi.org/10.1007/s12583-015-0523-1.
[106] L. Tian, J. Tong, Y. Xiao, M.J. Benton, H. Song, H. Song, L. Liang, K. Wu, D. Chu, T.J. Algeo, Environmental instability prior to end-Permian mass extinction reflected in biotic and facies changes on shallow carbonate platforms of the Nanpanjiang Basin (South China), Palaeogeogr. Palaeoclimatol. Palaeoecol. 519 (2019) 23–36, https://doi.org/10.1016/j.palaeo.2018.05.011.